Design and Performance of an Erbium-Doped Silicon Waveguide Detector Operating at 1.5 μm

P. G. Kik, A. Polman, S. Libertino, and S. Coffa

***Abstract*—A new concept for an infrared waveguide detector based on silicon is introduced. It is fabricated using silicon-on-insulator material, and consists of an erbium-doped p–n junction located in the core of a silicon ridge waveguide. The detection scheme relies on the optical absorption of 1.5-μm light by Er^{3+} ions in the waveguide core, followed by electron–hole pair generation by the excited Er and subsequent carrier separation by the electric field of the p–n junction. By performing optical mode calculations and including realistic doping profiles, we show that an external quantum efficiency of 10^{-3} can be achieved in a 4-cm-long waveguide detector fabricated using standard silicon processing. It is found that the quantum efficiency of the detector is mainly limited by free carrier absorption in the waveguide core, and may be further enhanced by optimizing the electrical doping profiles. Preliminary photocurrent measurements on an erbium-doped Si waveguide detector at room temperature show a clear erbium related photocurrent at 1.5 μm.**

***Index Terms*—Erbium, infrared detectors, integrated optoelectronics, semiconductor junctions, silicon, waveguides.**

I. Introduction

SILICON is an ideal material for the fabrication of optical waveguides that are compatible with optical telecommunication technology at 1.5 μm, because of its high transparency and high refractive index at this wavelength. The high transparency is due to the large mismatch between the 1.5-μm photon energy (0.8 eV) and the silicon bandgap energy (1.1 eV at room temperature). At the same time, the energy mismatch also excludes the fabrication of all-silicon active waveguide devices such as detectors and emitters operating at 1.5 μm. This problem may be solved by doping the silicon with small amounts of optically active erbium (Er) ions. In silicon, the rare earth ion Er^{3+} can be electrically excited and can subsequently emit 1.5-μm light due to an electronic transition in its incompletely filled $4f$ shell. Er-doped light-emitting diodes in Si operating at 1.5 μm have been made, with a quantum efficiency of up to 10^{-4} at room temperature [1]–[3]. Recently, we have found that the reverse process can also take place: an Er-doped Si p–n junction can generate a photocurrent when illuminated with 1.5-μm light [4]. This effect allows for the fabrication of a silicon photodetector that is sensitive at 1.5 μm.

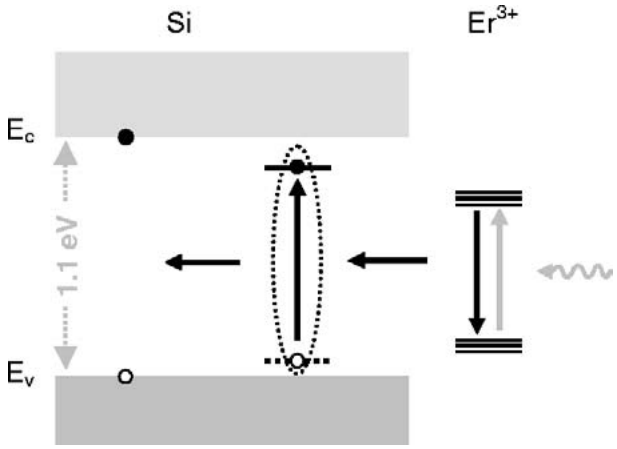

Fig. 1. Energy transfer processes in Er-doped silicon waveguide detector. An incoming photon excites and Er ion from the ground state into the first excited manifold. The excited Er ion decays by the creation of a exciton bound at the Er related defect site in Si. This exciton in turn can dissociate resulting in the generation of a free electron–hole pair. In a p–n junction geometry the carriers can be collected, leading to a net photocurrent at 1.534 μm.

Fig. 1 shows a schematic of this energy transfer mechanism. The Er related photoresponse at 1.5 μm is due to optical absorption within the Er $4f$ shell, followed by an interaction between the Er ion and the Si matrix. When Er in Si is optically excited from the ground state into the first excited manifold, it can de-excite and generate a localized electron–hole (e–h) pair trapped at the Er related defect site in Si [5]. This exciton can then dissociate, leading to the formation of free carriers. If this thermal upconversion process occurs near the depletion region of a p–n junction, the generated carriers produce a photocurrent. As was shown previously using a planar Er-doped p–n junction geometry [4], excited Er can generate electron–hole pairs with an efficiency as high as 70% at room temperature. However, due to the small optical absorption cross section of the Er ions and the limited width of the depletion region, the fraction of the light that is absorbed at normal incidence on such a p–n junction is very small ($\sim 10^{-7}$). To improve the absorption efficiency, a high Er concentration and a large interaction length are required. The maximum concentration of Er soluble in Czochralski grown silicon [6] is $\sim 10^{18}$ cm^{-3}. It can be further enhanced by co-doping with impurities such as oxygen [7], [8]. The interaction length of the light with the Er-doped junction can be increased by using a planar waveguide geometry, in which the p–n junction extends over the full length of

Manuscript received April 2, 2001; revised February 15, 2002. This work was supported in part by the research program of the Foundation for fundamental research on matter (FOM), supported by the Dutch organization for scientific research (NWO), and in part by the Dutch technology foundation STW and the ESPRIT program of the European Union (SCOOP: Silicon-compatible optoelectronics).

P. G. Kik was with FOM. Institute for Atomic and Molecular Physics, 1009 DB Amsterdam, The Netherlands. He is now with the Department of Applied Physics, California Institute of Technology, Pasadena, CA 91125 USA.

A. Polman is with FOM. Institute for Atomic and Molecular Physics, 1009 DB Amsterdam, The Netherlands (e-mail: polman@amolf.nl).

S. Libertino is with CNR-IMETEM, I-95121 Catania, Italy.

S. Coffa was with CNR-IMETEM, I-95121 Catania, Italy. He is now with STMicroelectronics, I-95121 Catania, Italy.

Publisher Item Identifier S 0733-8724(02)05122-8.

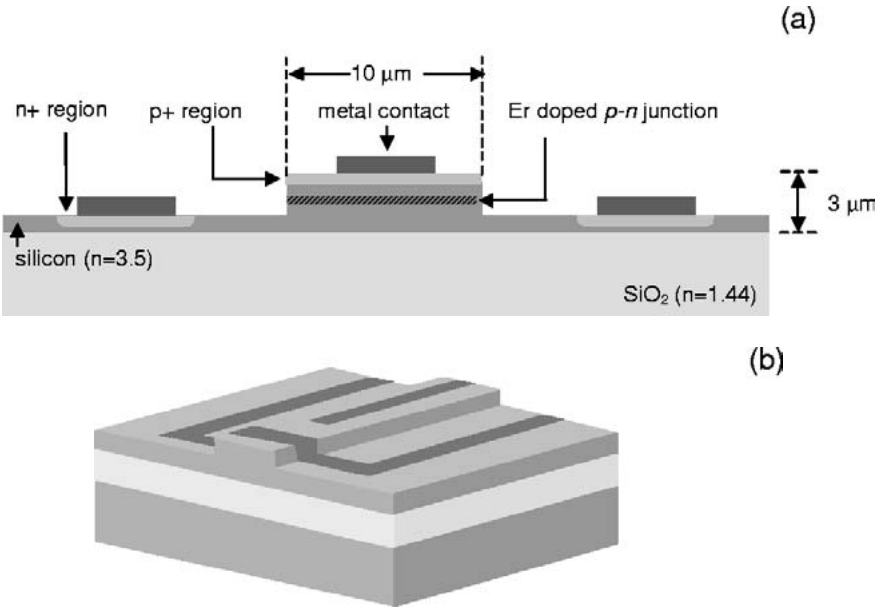

Fig. 2. (a) Schematic cross section of an Er-doped waveguide detector in Si. (b) Three-dimensional perspective view of the detector, also showing the layout of the metal contact strips (dark gray).

the waveguide. In this paper, we will describe the parameters that determine the performance of such a waveguide detector, and calculate the quantum efficiency that can be achieved. Finally, preliminary measurements of the photoresponse of such an Er-doped Si p–n junction waveguide detector are presented.

II. Device Layout

Fig. 2(a) shows a schematic cross section of the proposed waveguide detector structure. A three-dimensional perspective is shown in Fig. 2(b). The device is based on commercially available silicon-on-insulator (SOI) material, consisting of a thin crystalline Si top layer separated from the Si substrate by a SiO_2 layer. In this material, light can be confined in the high refractive index Si top layer ($n = 3.5$) by total internal reflection at the interface with air ($n = 1.0$) and with the SiO_2 layer ($n = 1.44$), provided that the SiO_2 is sufficiently thick to avoid coupling to the Si substrate. Lateral confinement is achieved by etching a ridge structure in the Si top layer [see Fig. 2(a)]. As an example, a ridge width of 10 μm and an etch depth of 2 μm are chosen, ensuring good optical mode confinement. The center of the waveguide is doped with Er. A p–n junction is formed near the waveguide center by means of a shallow boron implant into the n-type (lightly P doped) Si substrate layer. This also generates the p^+ region required for good electrical contact. The n^+ (highly P doped) side contacts are located 10 μm away from the waveguide core. Electrical contact is made via metal stripe contacts running over the n^+ ridge and p^+ side contact regions, as indicated in Fig. 2(b).

III. Contributions to the External Quantum Efficiency

The external quantum efficiency $\eta_{\rm ext}$ of the detector structure shown in Fig. 2 is determined by the fraction of the incoming light that is absorbed by the Er, and the conversion efficiency of excited Er to free e–h pairs $\eta_{\rm int}$, which in [4] was determined to be 70% at room temperature. This gives

$$\eta_{\rm ext} = \left(1 - e^{-\alpha_{\rm WG} \times L}\right) \frac{\alpha_{\rm Er}}{\alpha_{\rm WG}} \times \eta_{\rm int} \tag{1}$$

with $\alpha_{\rm Er}$ ($\rm cm^{-1}$) the absorption coefficient due to optical absorption at 1.5 μm by Er, $\alpha_{\rm WG}$ ($\rm cm^{-1}$) the total waveguide loss including absorption and scattering, and L (cm) the waveguide length. For a sufficiently long detector, $\eta_{\rm ext}$ is dominated by $\alpha_{\rm Er}/\alpha_{\rm WG}$, the ratio of the absorption by Er and the total waveguide loss.

Apart from the absorption loss, the waveguide loss $\alpha_{\rm WG}$ also contains scattering loss. It has been shown that a scattering loss below 0.5 dB/cm at 1.5 μm can be achieved in SOI waveguides [9]. Optical losses were measured on waveguides made on the same substrate as the detector structures, but without the highly doped layers and metal contacts; they amount to 1 dB/cm. In the quantum efficiency calculations, waveguide loss will be neglected. The remaining loss contributions in the waveguide detector are optical absorption by the Er ions, absorption by free carriers, and absorption by the metal contacts.

A. Absorption by the Metal Contacts

The presence of a contact on top of the ridge waveguide is required for current collection, but introduces strong absorption. For example, the absorption coefficient of aluminum at 1.5 μm is 1.3×10^6 $\rm cm^{-1}$ [10] which, in the geometry of Fig. 2, with a metal over the full length of the ridge, would cause the guided 1.5-μm light to be absorbed within 100 μm. In order to reduce this effect, first of all, the metal length could be optimized. Depending on the series resistance, and for small photocurrent, the n^+ layer itself could act as the main current conducting path, and only small sized metals pads would be required to collect the current from the device. To further reduce absorption by the top metal contact, the light intensity near the top of the ridge

should be reduced. This can be achieved by lowering the effective index just below the top contact, e.g., by performing an additional etch to narrow the top region of the waveguide core, or by partial oxidation of the ridge below the metal contact. Ideally, a thick oxide between metal and Si waveguide would solve the coupling problem, but at the same time it deteriorates the electrical performance. Alternatively, a transparent conductive layer, e.g., indium–tin–oxide optimized for 1.5-μm transmission, may be used as a buffer layer between the metal contact and the waveguide core. Since absorption by the top contact is not intrinsic to the detection scheme, it is not included in the following quantum efficiency calculations.

B. Optical Absorption by Er

The magnitude of the Er related optical absorption in the waveguide detector structure is given by $\alpha_{\mathrm{Er}} = \sigma_{\mathrm{Er}} \times C_{\mathrm{Er,\,peak}} \times \Gamma_{\mathrm{Er}}$ with $\sigma_{\mathrm{Er}} = 1.8 \times 10^{-20}$ cm^2 the optical absorption cross section of Er at 1.5 μm as determined in [4], $C_{\mathrm{Er,\,peak}}$ (cm^{-3}) the Er peak concentration, and Γ_{Er} the effective overlap of the Er concentration profile with the intensity distribution in the waveguide core. To optimize the mode overlap, the Er should be located near the center of the waveguide. The optimum Er concentration will be discussed in Section VI.

C. Free Carrier Absorption

Free electrons and holes in silicon can be excited higher in their respective bands by absorption of sub-bandgap radiation. This free carrier absorption occurs inside the waveguide core due to three sources of electrical carriers: free electrons from the n-type Si waveguide layer (α_n), free holes in the p$^+$ top contact ($\alpha_{\mathrm{P+}}$), and Er related free electrons in the center of the waveguide ($\alpha_{\mathrm{Er,\,e}}$) which are present due to the donor character of Er [11]. The cross sections for optical absorption by free electrons and holes are 9.5×10^{-18} cm^2 and 6.4×10^{-18} cm^2, respectively [12]. Note that these cross sections are two orders of magnitude larger than the cross section for optical absorption by Er. Consequently, for optimum detector performance the overlap of the intensity profile with the highly doped p$^+$ contact should be kept as small as possible.

IV. Numerical Calculations

Calculations of the detector performance were made for the detector layout shown in Fig. 2. In the calculations, a 70-keV boron implant to a fluence of 10^{14} cm^{-2} was used for the p$^+$ top contact formation, and the n-type background doping was taken to be 2×10^{15} cm^{-3} (corresponding to a resistivity of 2 Ω·cm). The Er implantation energy was chosen such that the Er was placed in the center of the waveguide core (5 MeV) and the Er fluence was 10^{13} cm^{-2}. This fluence is sufficiently low to prevent amorphization of the Si, avoiding Er segregation [8] during the thermal annealing that is required to activate the Er.

Fig. 3(a) shows the resulting free carrier distributions and the Er distribution as a function of y-position in the waveguide core, with $y = 0$ μm corresponding to the Si–SiO$_2$ interface and $y = 3$ μm corresponding to the top of the ridge. Indicated are the hole distribution in the p$^+$ contact (▷), the Er concentration profile (●), the Er induced electron concentration (○), which is taken to be 10% of the Er concentration assuming 10% electrical activation [11], and the n-type background doping (dotted line). The depletion region induced by these doping profiles extends from $y = 1.7$ to $y = 2.1$ μm as indicated by the dark gray area, and contains approximately 30% of the implanted Er.

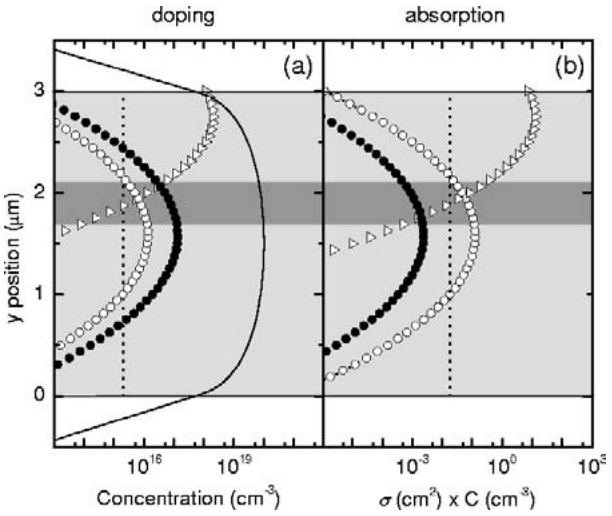

Fig. 3. (a) Concentration depth profiles at $x = 0$ (center of the ridge) for boron (▷), erbium (●), and the Er induced free carrier (electron) concentration (○), for the device layout in Fig. 1. The n-type substrate doping is indicated by the dotted line, and the calculated TE(0,0) mode intensity for $\lambda = 1.5$ μm is indicated by the solid line. The light gray region represents the waveguide core, and the dark gray region represents the depletion region formed at the p–n junction. In this region, free carrier absorption is strongly reduced. (b) Local absorption coefficient for each of the individual curves in (a), obtained by multiplying the curves in (a) with the corresponding absorption cross sections, as listed in Table I.

The requirement of low intensity in the p$^+$ region and high intensity at the Er-doped center of the waveguide core is optimally fulfilled by zeroth-order optical modes. Higher order modes would experience larger absorption. The intensity distributions of the zeroth-order transverse electric mode TE(0,0) and the zeroth-order transverse magnetic mode TM(0,0) at 1.5 μm were calculated using a finite difference method. The calculated TE(0,0) intensity distribution at $x = 0$ is included in Fig. 3(a) (solid line). Due to the large core size, almost all power is confined within the Si core. The TM(0,0) mode has an almost identical intensity distribution, with a slightly lower intensity at the top and bottom interfaces.

In order to compare the magnitude of the different absorption contributions to the total absorption, we have multiplied the concentrations in Fig. 3(a) by the corresponding absorption cross sections (see Table I). These data are shown in Fig. 3(b), using the same symbols as in Fig. 3(a). This plot clearly shows that in the present geometry optical absorption by Er is only a small contribution to the total absorption. However, since the interaction between the separate doping profiles generates a depletion region, in part of the waveguide the optical absorption by Er will dominate. The total detector response will thus be determined by absorption in this region, relative to the free carrier absorption losses outside this region.

In order to estimate the absorption of zeroth-order modes, we have determined the overlap Γ of the normalized optical modes with the peak-normalized dopant distributions. In the case of

TABLE I
OPTICAL ABSORPTION CROSS SECTIONS AND PEAK CONCENTRATIONS USED IN THE QUANTUM EFFICIENCY CALCULATIONS, AS WELL AS THE CALCULATED MODE OVERLAP AND ABSORPTION COEFFICIENTS

	σ (cm^2)	C_{peak} (cm^{-3})	Γ^{TE} (%)	α^{TE} (cm^{-1})	Γ^{TM} (%)	α^{TM} (cm^{-1})
α_{Er}	1.8×10^{-20}	1.4×10^{17}	43	0.0011	44	0.0011
$\alpha_{Er,e}$	9.5×10^{-18}	1.4×10^{16}	29	0.039	31	0.041
α_n	9.5×10^{-18}	2×10^{15}	79	0.015	79	0.015
α_{p+}	6.4×10^{-18}	2×10^{18}	5.2	0.65	4.4	0.56

free carrier absorption, we have taken into account the absence of free carriers in the depletion region of the (unbiased) p–n junction. These data, listed in Table I, together with the known peak concentrations $C_{\rm peak}$ of the distributions and the relevant cross sections σ give the separate contributions to the total absorption according to $\alpha = \sigma \times C_{\rm peak} \times \Gamma$. The results are summarized in Table I. The main contribution to the absorption is found to be free carrier absorption by holes in the top contact [$\alpha_{\rm p+} = 0.65\ {\rm cm}^{-1}$ and $\alpha_{\rm p+} = 0.56\ {\rm cm}^{-1}$ for the TE(0,0) and TM(0,0) modes, respectively], even though the mode overlap with these carriers is only 4%–5%.

From the results in Table I, we find that the total waveguide absorption of the detector structure shown in Fig. 1 is $\alpha_{\rm WG} = 0.71\ {\rm cm}^{-1}$ and $\alpha_{\rm WG} = 0.62\ {\rm cm}^{-1}$ for the TE(0,0) and TM(0,0) modes, respectively. This implies that more than 90% of the guided light is absorbed in a 4-cm-long waveguide. The fraction of the TE and TM modes absorbed by the Er is 1.5×10^{-3} and 1.8×10^{-3}, respectively. Together with the known $\eta_{\rm int}$ of 70%, and assuming an electron–hole collection efficiency of 1, we find an external quantum efficiency of 10^{-3} for a 4-cm-long waveguide detector. This is three orders of magnitude higher than what was measured previously in a planar Er-doped p–n junctions illuminated at normal incidence [4], which is due to the strongly increased interaction length that can be achieved in a waveguide geometry.

V. PRELIMINARY MEASUREMENTS

An Er-doped Si p–n junction waveguide detector was fabricated according to the layout in Fig. 2, using a 3-MeV Er implant to a fluence of $10^{13}\ {\rm cm}^{-2}$, a 40-keV B implant to a fluence of $10^{14}\ {\rm cm}^{-2}$, and a total waveguide length of 5 mm. These conditions, though somewhat different from those used in the simulations, were identical to those used in the planar p–n junction experiments described in [4]. Fig. 4 shows the current–voltage (I–V) characteristic of the detector. The detector exhibits an open circuit voltage of 0.7 V, and the ideality factor is 1.33. The saturation current calculated from a fit of the forward bias data is $42 \pm 5\ \mu{\rm A/cm}^2$, while the measured dark current at -1 V equals $630\ \mu{\rm A/cm}^2$. This indicates there is significant leakage across the junction. Photocurrent measurements at room temperature were performed by coupling the output of a tunable diode laser ($\lambda_{em} = 1.51$–$1.57\ \mu$m) into the detector waveguide, using a single-mode tapered fiber. The laser signal was mechanically chopped at 267 Hz and the photocurrent was measured using lock-in detection. The collected current was converted to external quantum efficiency $\eta_{\rm ext}$ by dividing the collected photocurrent by the 1.5-μm photon flux in the input fiber measured using a calibrated detector. Hence, $\eta_{\rm ext}$ also includes the fiber-to-waveguide coupling efficiency. From measurements on similar waveguides, a coupling loss of 7 dB was found.

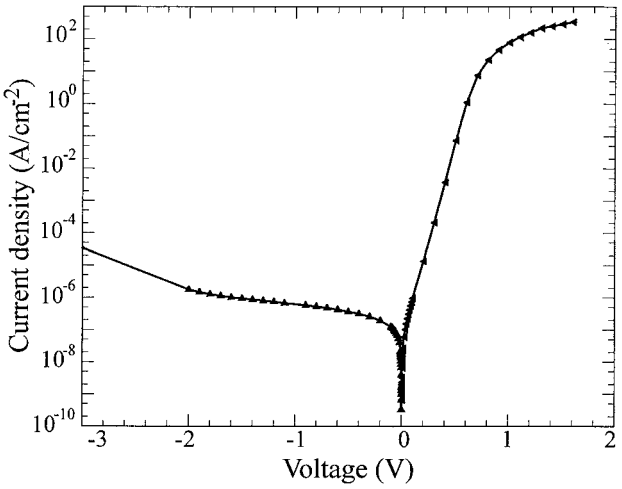

Fig. 4. Current–voltage characteristic of an Er-doped waveguide detector fabricated in silicon-on-insulator material using standard silicon processing technology.

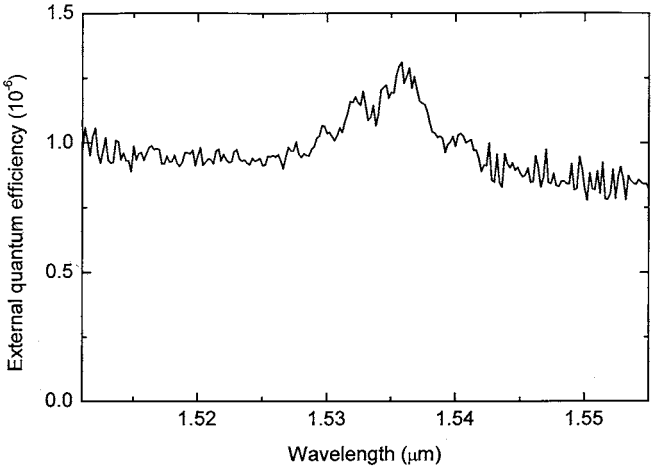

Fig. 5. Photoresponse of an Er-doped waveguide detector fabricated in silicon-on-insulator material using standard silicon processing technology, showing an Er related photocurrent at 1.54 μm.

Fig. 5 shows the thus obtained $\eta_{\rm ext}$ as a function of wavelength, measured at a forward bias of 0.4 V. The spectrum shows a peak centered around 1.535 nm superimposed on a rather constant signal. The peak is attributed to the main ${}^4I_{15/2} \rightarrow {}^4I_{13/2}$ absorption transition in Er^{3+}. The background is due to a broad

range of absorption transitions within the Er Stark manifolds (see e.g., [13]), as well as photocurrent attributed to optical transitions related to implantation damage in the p–n junction. Given the known shape of the Er absorption spectrum and the spectral shape in Fig. 5, it can be concluded that both these components are roughly equal in strength. The Er related photocurrent was found to be roughly independent of the bias conditions, while the defect background current increased by a factor of 14 upon increasing the reverse bias from 0 to 5 V. This increase may be related to the spatial distribution of the Er induced implantation damage, which is expected to be mostly located at the end-of-range of the Er implantation profile: as the reverse bias is increased the depletion region reaches the defect rich region, possibly leading to a large defect related current. Note that the defect related current generation mechanism could also be considered as a candidate for a Si-based infrared detector.

The observed external quantum efficiency $\eta_{\text{ext}} \sim 1 \times 10^{-6}$ is much lower than the value calculated in Section IV, which is attributed to the strong absorption of the aluminum top contact. The absorption of the TE(0,0) mode by the top contact is estimated to be $\alpha_{TC} \approx 10^2$ cm^{-1} using the calculated mode overlap of 9×10^{-5} and the absorption coefficient of bulk aluminum. Taking this absorption into account, the maximum η_{ext} that can be obtained in the present detector design is 7×10^{-6}, which is somewhat higher than observed. Most of this difference can be directly related to coupling losses.

VI. Device Optimization

The previous sections clearly demonstrated the viability of an Er-doped silicon infrared waveguide detector, both theoretically and experimentally. Several design improvements can be implemented. First, the free carrier absorption could be reduced by reducing the electrical doping levels. The minimum carrier concentration that can be used is determined by the field required for efficient charge separation. This sets a limit to the doping levels on either side of the Er-doped core region.

Second, the detector efficiency may be enhanced by increasing the amount of Er in the waveguide core. This, however, also has a number of undesired consequences. First, because of the donor character of Er, the absorption by Er induced electrons increases. As can be seen from Table I, increasing the Er concentration by a factor of 10 generates an Er related free carrier absorption with a magnitude similar to $\alpha_{\text{p+}}$, which significantly influences the quantum efficiency. Incorporation of large concentrations of erbium may also introduce undesired crystal damage [7], which increases the carrier recombination rate and reduces the collection efficiency.

The combination of a good crystal quality and a high Er concentration has only been achieved by the use of oxygen co-doping and high temperature anneals [7]. Unfortunately, these are also the conditions that lead to a high Er donor activity (up to 80%) [7]. Consequently, further experiments are required to find the appropriate impurity co-doping and annealing conditions for optimum detector performance. Note that most studies of the incorporation of Er in Si have focused on optimizing the Er luminescence intensity and reducing the thermal quenching of the intensity. The thus obtained "optimized" processing conditions may be nonideal for the desired current generation process.

The proposed detector length of 4 cm may be impractical for integration within optoelectronic integrated circuits. However, due to the high refractive index of silicon, it is possible to create low-loss waveguide bends with a bending radius on the order of 1 μm [14]. This makes it possible to "roll up" a 4-cm-long waveguide spiral to an area of 2 mm^2 (assuming 40-μm waveguide spacing). Another issue related to the device dimensions is the junction capacitance. The junction area of the 4-cm-long waveguide, given by the product of the ridge width and the waveguide length, is 0.4 mm^2. The capacitance associated with such a large p–n junction limits the detector response time. This problem may be solved by "photon recycling," i.e., by designing a waveguide structure in which light makes multiple passes through a smaller p–n junction. A simple design could involve a Bragg reflector at the waveguide end which reflects remaining 1.5-μm light back into the detector, reducing the required waveguide length by a factor of 2. More sophisticated designs may include microring resonators and waveguide microcavities [15]. Eventually, the optimum detector response time will be determined by the rate limiting step in the energy transfer process from Er to the Si electronic system, which in [4] was determined to be 2×10^6 s^{-1}. Detectors with such a response time could, e.g., find applications in all-optical interconnects used to electrically isolate the driver circuits from Si-based high-power diodes and transistors, which typically operate at frequencies of 10 kHz.

VII. Conclusion

A new concept of an Er-doped silicon infrared waveguide detector is introduced. It consists of a silicon ridge waveguide containing an Er-doped p–n junction along the waveguide length. The detection scheme is based on an energy conversion scheme in which the excitation energy of optically excited Er is transferred to the Si electronic system, inducing a photocurrent under 1.5-μm illumination. From optical mode calculations, it is concluded that an external quantum efficiency of 10^{-3} can be achieved in a 4-cm-long waveguide structure. It is shown that free carrier absorption is an intrinsic limiting factor for the external quantum efficiency. Optimization of the detector design should therefore focus on obtaining optimum overlap of the Er doping profile with the depletion region and minimum overlap of the optical modes with free carriers in the waveguide. Preliminary measurements on an Er-doped waveguide detector in silicon indeed show an Er related photocurrent at 1.5 μm.

Acknowledgment

The authors would like to acknowledge N. Hamelin for some of the initial design calculations.

References

[1] G. Franzò, F. Priolo, S. Coffa, A. Polman, and A. Carnera, "Room-temperature electroluminescence from Er-doped crystalline Si," *Appl. Phys. Lett.*, vol. 64, pp. 2235–2237, Apr. 1994.

[2] B. Zheng, J. Michel, F. Y. G. Ren, L. C. Kimerling, D. C. Jacobson, and J. M. Poate, "Room-temperature sharp line electroluminescence at $\lambda = 1.54\,\mu$m from an erbium-doped, silicon light-emitting diode," *Appl. Phys. Lett.*, vol. 64, pp. 2842–2844, May 1994.

[3] S. Coffa, G. Franzò, and F. Priolo, "High efficiency and fast modulation of Er-doped light emitting Si diodes," *Appl. Phys. Lett.*, vol. 69, pp. 2077–2079, Sept. 1996.
[4] N. Hamelin, P. G. Kik, J. F. Suyver, K. Kikoin, A. Polman, A. Schönecker, and F. W. Saris, "Energy backtransfer and infrared photoresponse in erbium-doped silicon p–n diodes," *J. Appl. Phys.*, vol. 88, pp. 5381–5387, Nov. 2000.
[5] S. Libertino, S. Coffa, G. Franzò, and F. Priolo, "The effects of oxygen and defects on the deep-level properties of Er in crystalline Si," *J. Appl. Phys.*, vol. 78, pp. 3867–3873, Sept. 1995.
[6] D. J. Eaglesham, J. Michel, E. A. Fitzgerald, D. C. Jacobson, J. M. Poate, J. L. Benton, A. Polman, Y.-H. Xie, and L. C. Kimerling, "Microstructure of erbium-implanted Si," *Appl. Phys. Lett.*, vol. 58, pp. 2797–2799, June 1991.
[7] S. Coffa, F. Priolo, G. Franzò, V. Bellani, A. Carnera, and C. Spinella, "Optical activation and excitation mechanisms of Er implanted in Si," *Phys. Rev. B*, vol. 48, pp. 11 782–1788, Oct. 1993.
[8] J. S. Custer, A. Polman, and H. M. van Pinxteren, "Erbium in crystal silicon: Segregation and trapping during solid phase epitaxy of amorphous silicon," *J. Appl. Phys.*, vol. 75, pp. 2809–2817, Mar. 1994.
[9] J. Schmidtchen, A. Splett, B. Schuppert, K. Petermann, and G. Burbach, "Low-loss singlemode optical wave-guides with large cross-section in silicon-on-insulator," *Electron. Lett.*, vol. 27, pp. 1486–1488, Aug. 1991.
[10] E. D. Palik, *Handbook of Optical Constants of Solids*. Boston, MA: Academic, 1991.
[11] J. L. Benton, J. Michel, L. C. Kimerling, D. C. Jacobson, Y. H. Xie, D. C. Eaglesham, E. A. Fitzgerald, and J. M. Poate, "The electrical and defect properties of erbium-implanted silicon," *J. Appl. Phys.*, vol. 70, pp. 2667–2671, Sept. 1991.
[12] M. A. Green, "Silicon solar cells," University of New South Wales, Sydney, Australia, p. 48, 1995.
[13] M. J. Keevers, F. W. Saris, G. C. Zhang, J. Zhao, M. A. Green, and R. Elliman, "Screening of optical dopants in silicon solar cells for improved infrared response," in *Proc. 13th Eur. Photovoltaic Solar Energy Conf.*, Nice, France, Oct. 1995, pp. 1041–1044.
[14] A. M. Agarwal, L. Liao, J. S. Foresi, M. R. Black, X. Duan, and L. C. Kimerling, "Low-loss polycrystalline silicon waveguides for silicon photonics," *J. Appl. Phys.*, vol. 80, pp. 6120–6123, Dec. 1996.
[15] J. S. Foresi, P. R. Villeneuve, J. Ferrera, E. R. Thoen, G. Steinmeyer, S. Fan, J. D. Joannopoulos, L. C. Kimerling, H. I. Smith, and E. P. Ippen, "Photonic crystals: Putting a new twist on light," *Nature*, vol. 390, pp. 143–149, Mar. 1997.

P. G. Kik did his Ph.D. research at the F.O.M. Institute for Atomic and Molecular Physics, Amsterdam, The Netherlands, working with Prof. A. Polman. He is currently a Postdoctoral Scholar in the Department of Applied Physics at the California Institute of Technology in Pasadena, working with Prof. H.A. Atwater.

A. Polman is a Scientific Group Leader and Head of the Optoelectronic Materials Department at the F.O.M. Institute for Atomic and Molecular Physics, Amsterdam, The Netherlands.

S. Libertino is a researcher at the CNR-IMETEM, Catania, Italy. Her research fields include the design and characterization of Si-based optoelectronic devices; the integration of biological materials in Si-based hybrid devices. She has co-authored more than 40 papers and has two patents.

S. Coffa is the leader of Si Optoelectronics, Bio- and Nano-Systems at Corporate R&D of STMicroelectronics, Catania, Italy.